Supporting Information

Vertically Aligned MoS_2 Thin Film Catalysts with Fe-Ni Sulfide Nanoparticles by One-Step Sulfurization for Efficient Solar Water Reduction

Seokhoon Choi[1†], Changyeon Kim[1†], Jae Yoon Lee[2†], Tae Hyung Lee[1], Ki Chang Kwon[1], Sungwoo Kang[1], Sol A Lee[1], Kyoung Soon Choi[3], Jun Min Suh[1], Kootak Hong[1], Sang Eon Jun[1], Woo Kyoung Kim[4], Sang Hyun Ahn[5], Seungwu Han[1], Soo Young Kim[6], Chul-Ho Lee[2*], and Ho Won Jang[1*]*

[1] Department of Materials Science and Engineering, Research Institute of Advanced Materials, Seoul National University, Seoul 08826, Republic of Korea

[2] KU-KIST Graduate School of Converging Science and Technology, Korea University, Seoul 02841, Republic of Korea

[3] National research Facilities & Equipment Center (NFEC), Korea Basic Science Institute (KBSI), Daejeon 34133, Republic of Korea

[4] School of Chemical Engineering, Yeungnam University, Gyeongsan 38541, Republic of Korea

[5] School of Chemical Engineering and Material Science, Chung-Ang University, Seoul 06974, Republic of Korea

[6] Department of Materials Science and Engineering, Korea University, Seoul 02841, Republic of Korea

[*]Corresponding authors
E-mail: sooyoungkim@korea.ac.kr, chlee80@korea.ac.kr, hwjang@snu.ac.kr

[†] These authors contributed equally.

Keywords: Molybdenum disulfide; vertically aligned; photoelectrochemical; hydrogen evolution

reaction; silicon photocathode.

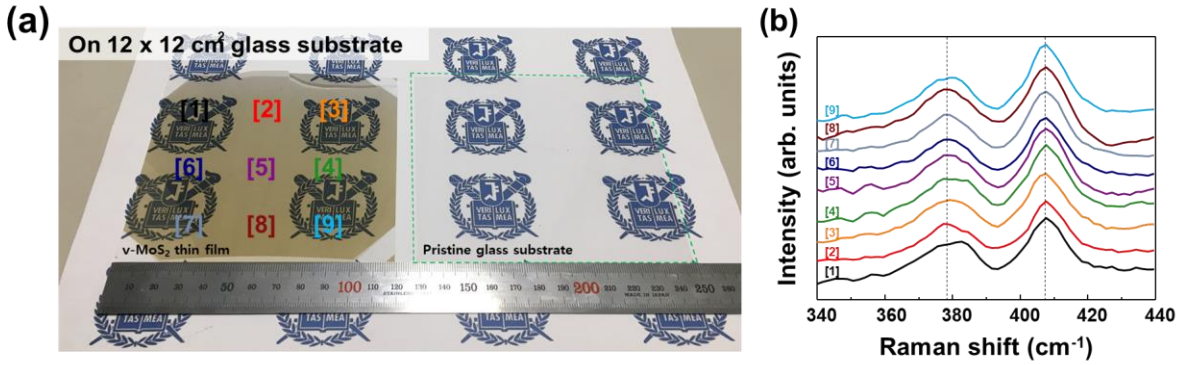

Fig. S1 (**a**) Photograph of synthesized VMS thin films on flexible and bare flexible glass substrate. (**b**) Raman spectra of synthesized VMS thin films on flexible glass substrate at each site.

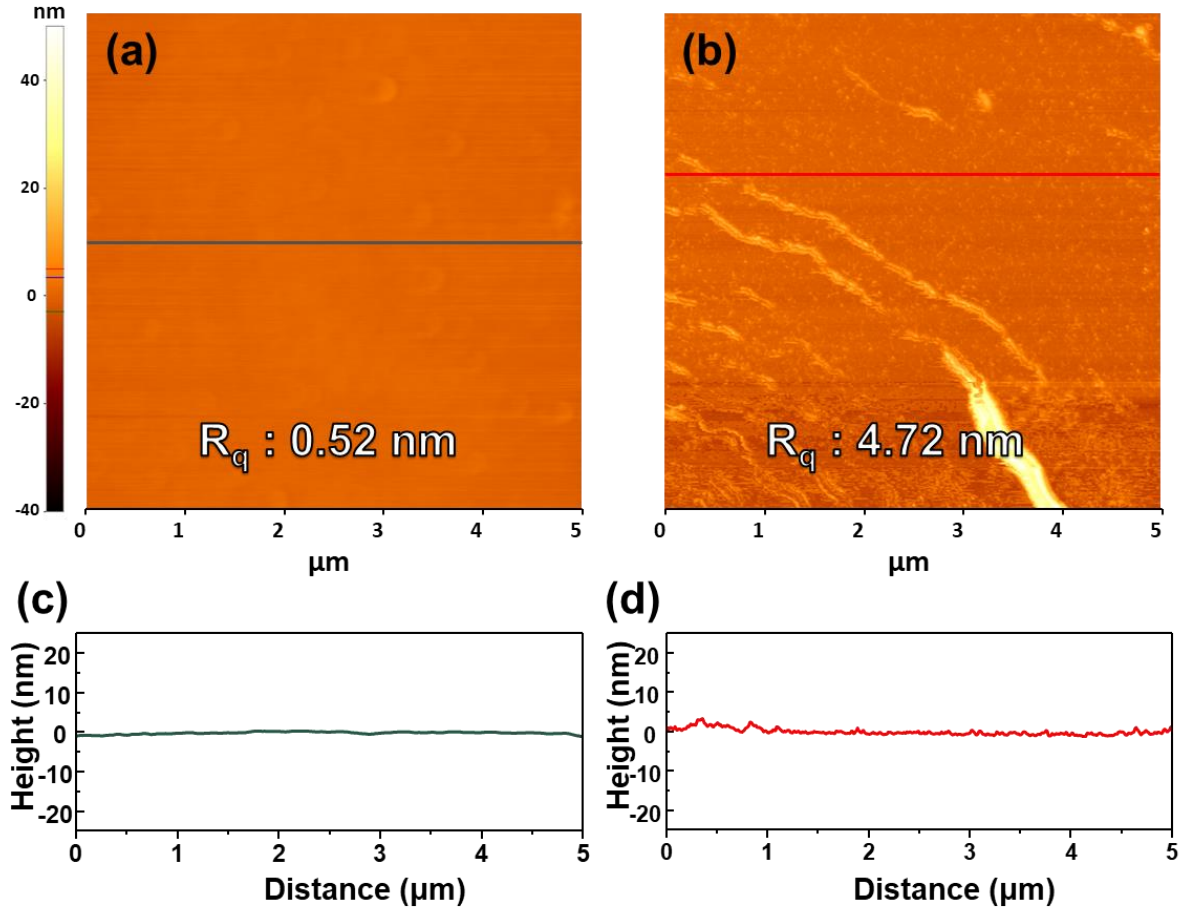

Fig. S2. AFM images of (**a**) PMS and (**b**) VMS. (**c**) corresponding line profiles of height along the green line in (a). (**d**) Corresponding line profiles of height along the red line in (b).

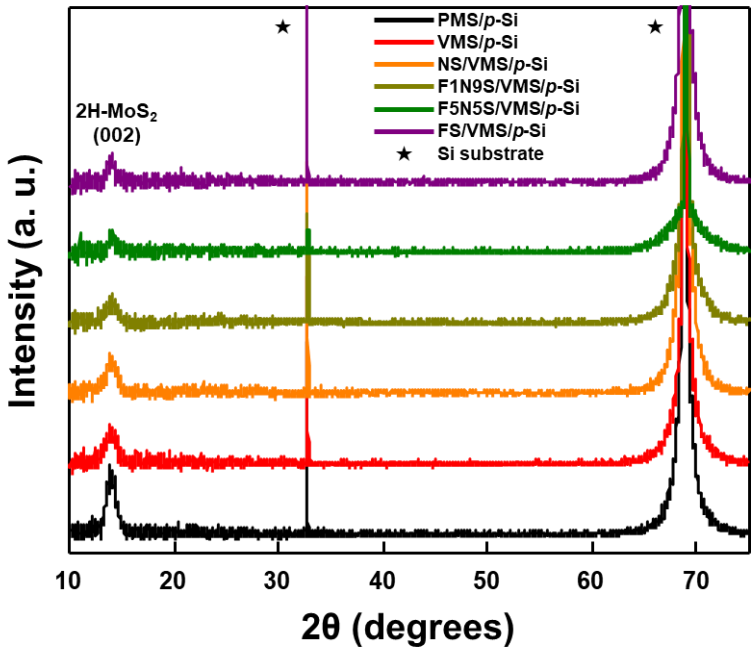

Fig. S3. X-ray diffraction patterns of synthesized thin films.

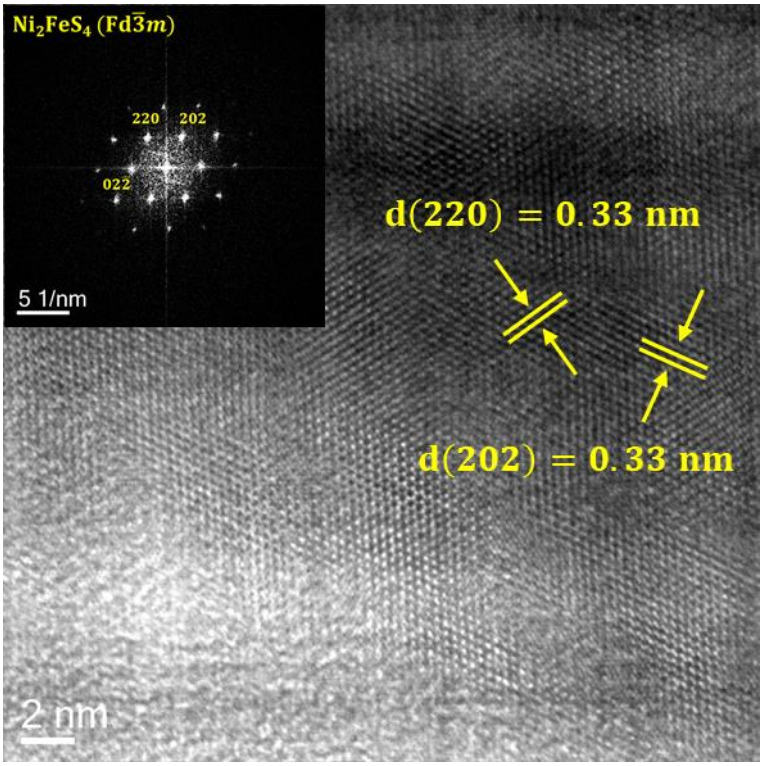

Fig. S4. The rarely found Ni_2FeS_4 phase in high-resolution TEM images of F1N9S/VMS thin film.

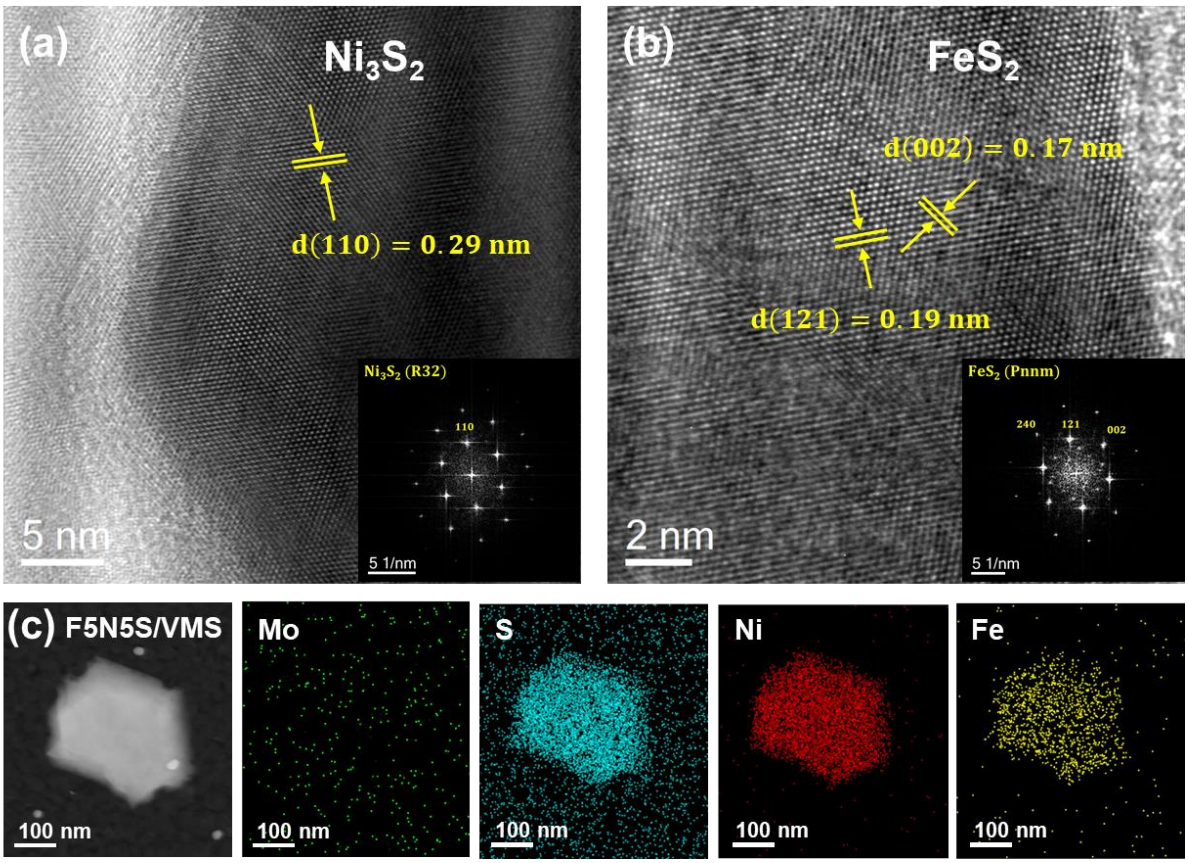

Fig. S5. High resolution TEM images of (**a**) F1N9S/VMS and (**b**) F5N5S/VMS thin films. (**c**) HAADF-STEM image and EDS mapping of F5N5S/VMS thin film.

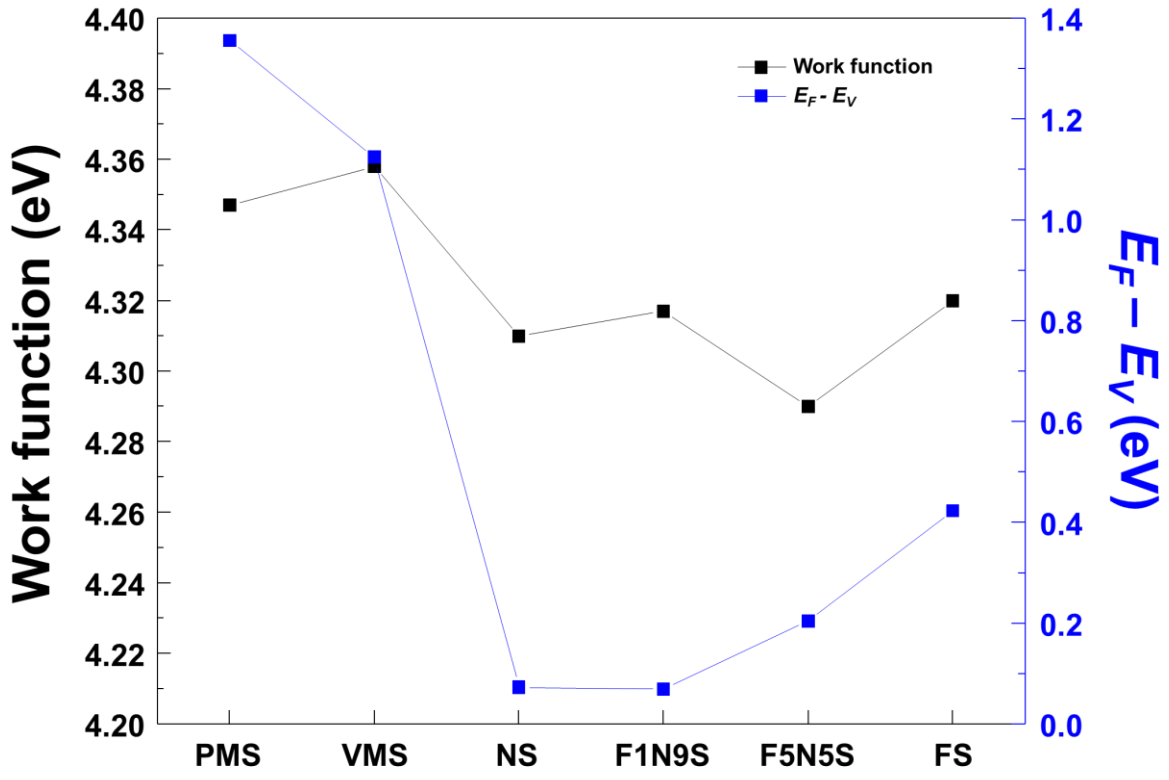

Fig. S6. Calculated work function and E_F - E_V values of PMS/*p*-Si, VMS/*p*-Si, and FNS NPs/*p*-Si photocathodes.

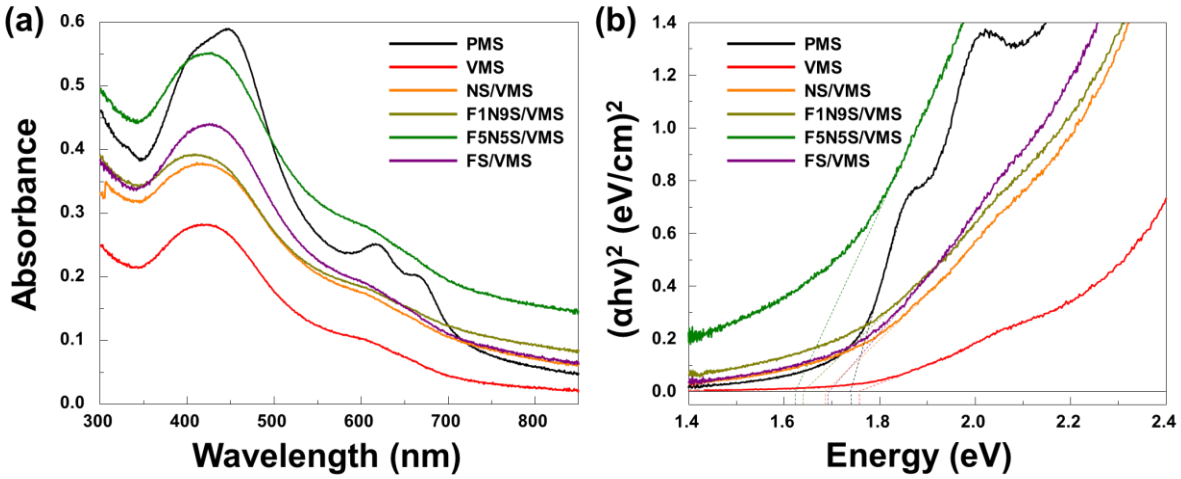

	PMS	VMS	NS/VMS	F1N9S/VMS	F5N5S/VMS	FS/VMS
Optical band gap (eV)	1.736	1.756	1.686	1.638	1.623	1.694

Fig. S7. (**a**) Absorbance spectra and (**b**) Tauc plots of PMS, VMS, NS/VMS, F1N9S/VMS, F5N5S/VMS, and FS/VMS thin film catalysts.

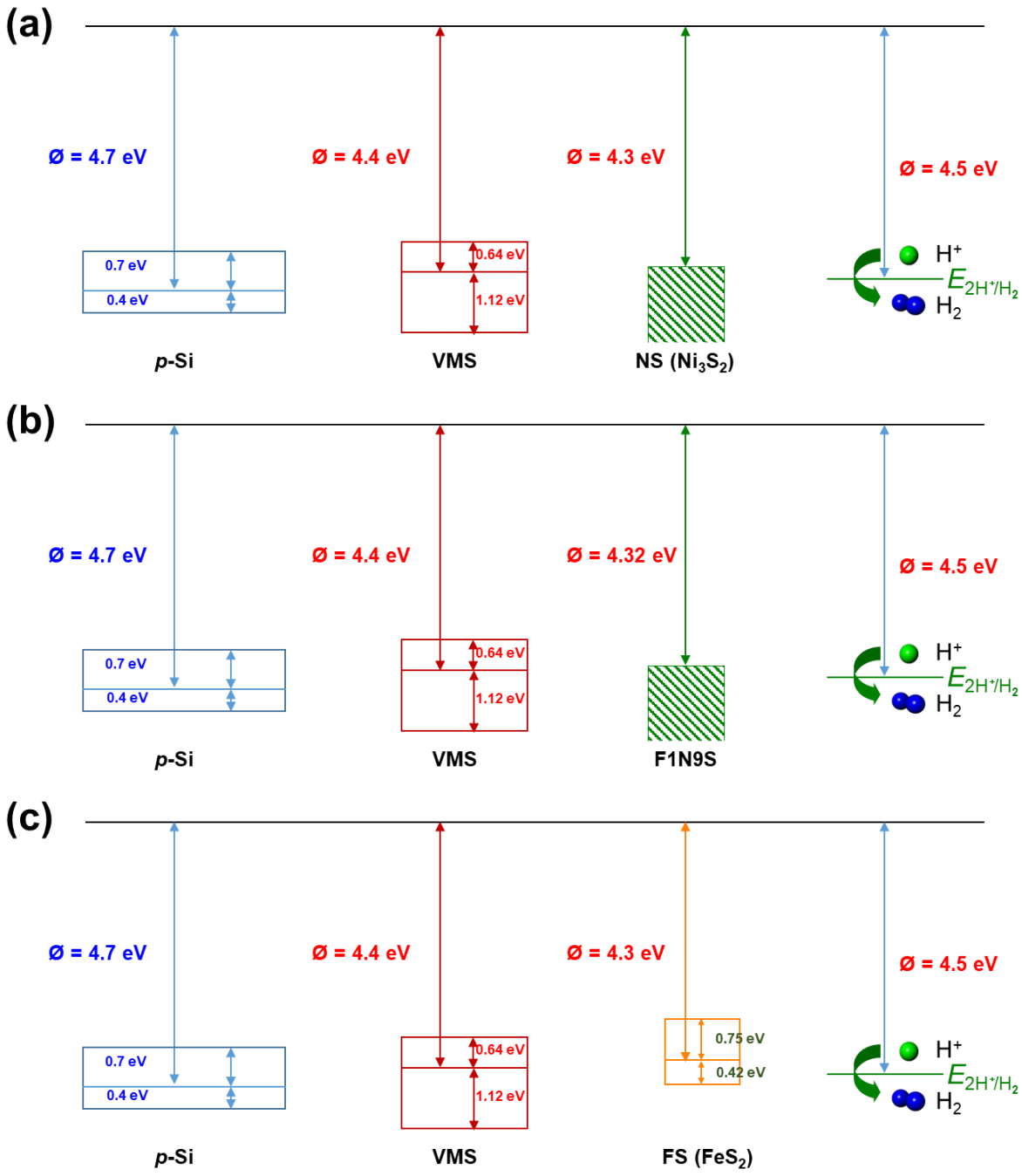

Fig. S8. (**a**) Flat band diagram of NS/VMS/*p*-Si. (**b**) Flat band diagram of F1N9S/VMS/*p*-Si. (**c**) Flat band diagram of FS/VMS thin film photocathodes.

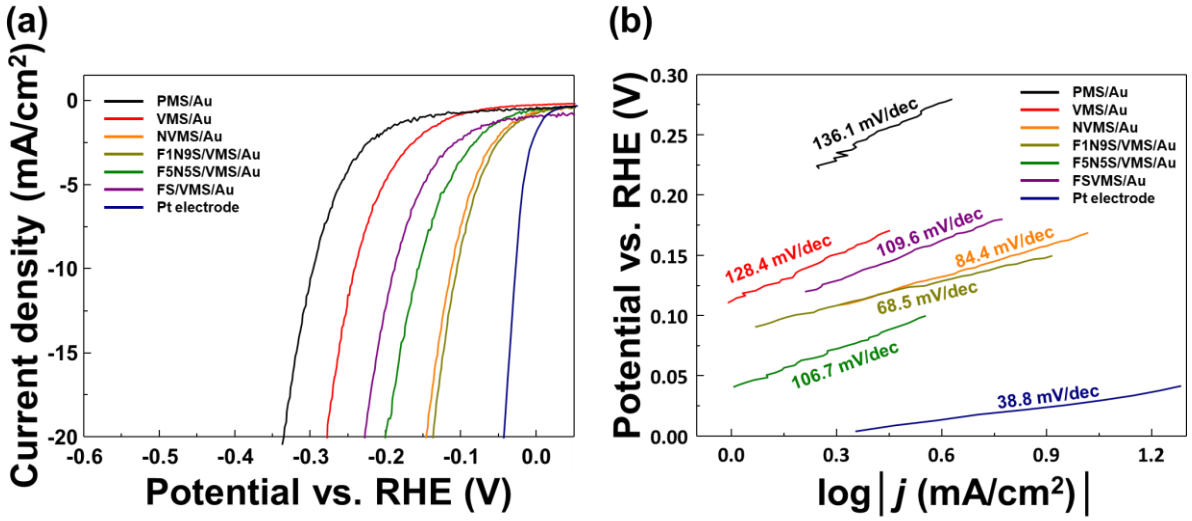

Fig. S9. (**a**) The polarization curves of the synthesized thin films on Au electrode. (**b**) Tafel slopes of the synthesized thin films plotted as log (j) against potential *vs*. RHE

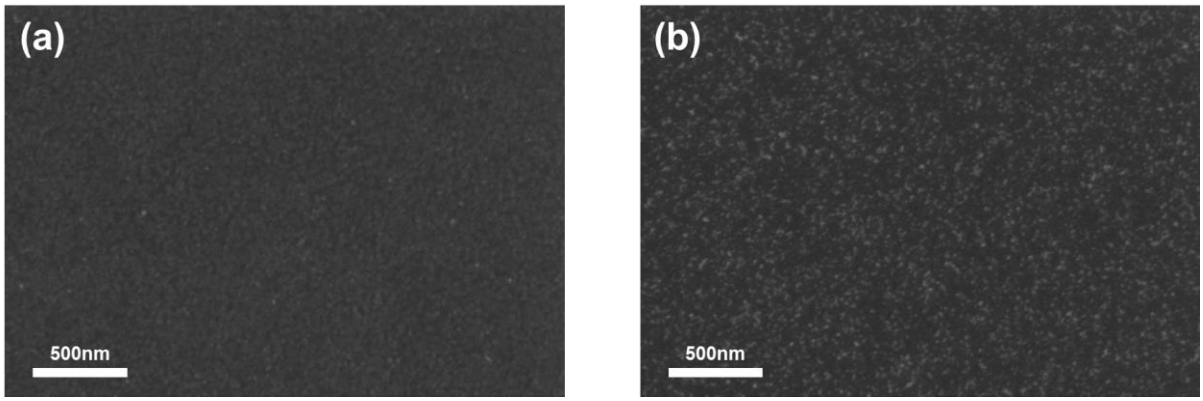

Fig. S10. SEM images of PMS/*p*-Si photocathode (**a**) before and (**b**) after morphological changes.

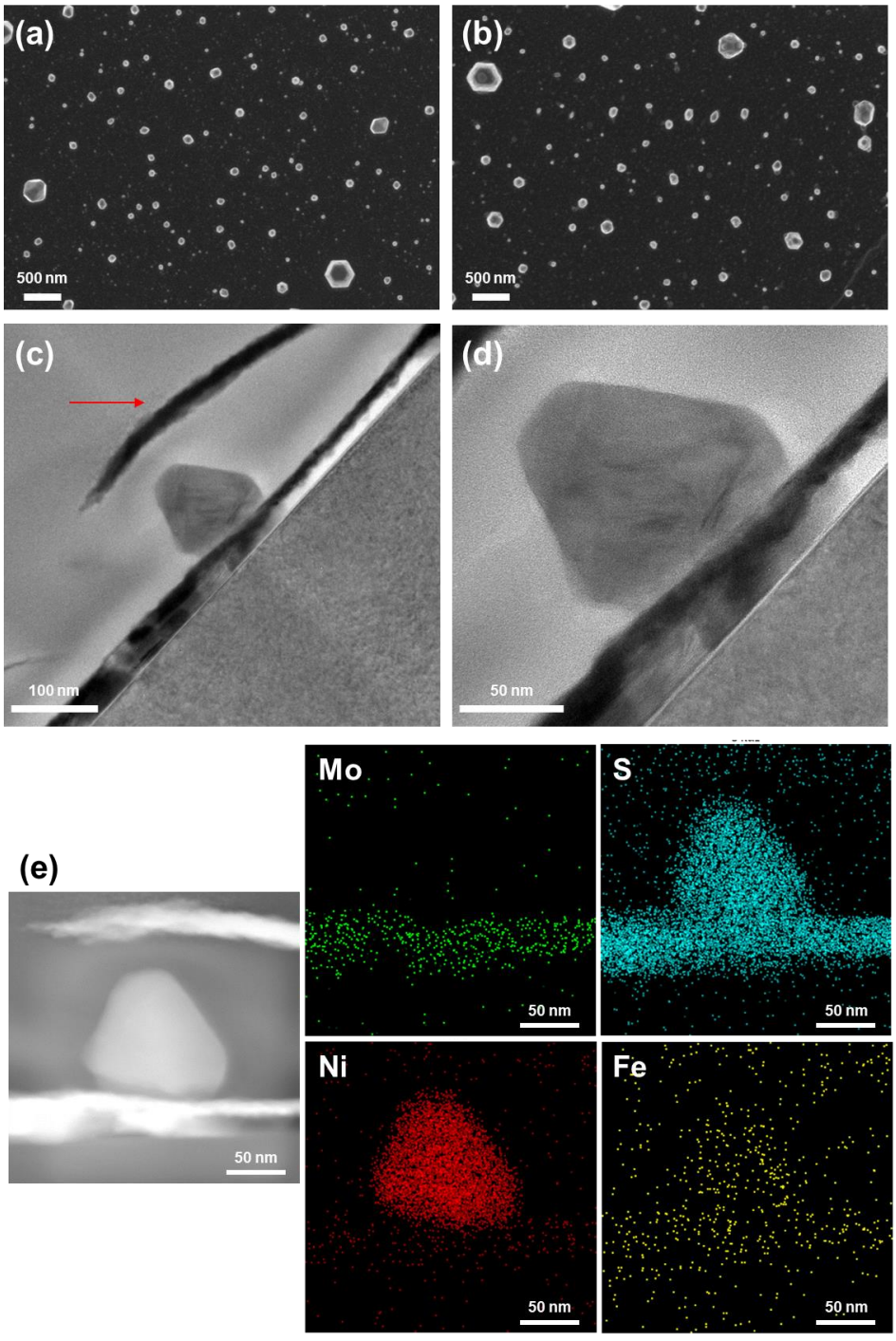

Fig. S11. SEM images of F1N9S/VMS/*p*-Si photocathode (**a**) before and (**b**) after the stability test. (**c**-**d**) TEM images of the F1N9S/VMS/*p*-Si photocathode after the stability test. Red arrow: deposited Ga layer during TEM sample preparation using focused ion beam (FIB) instrument. (**e**) Cross-sectional HAADF-STEM image and EDS mapping of F1N9S/VMS/*p*-Si photocathode after the stability test.

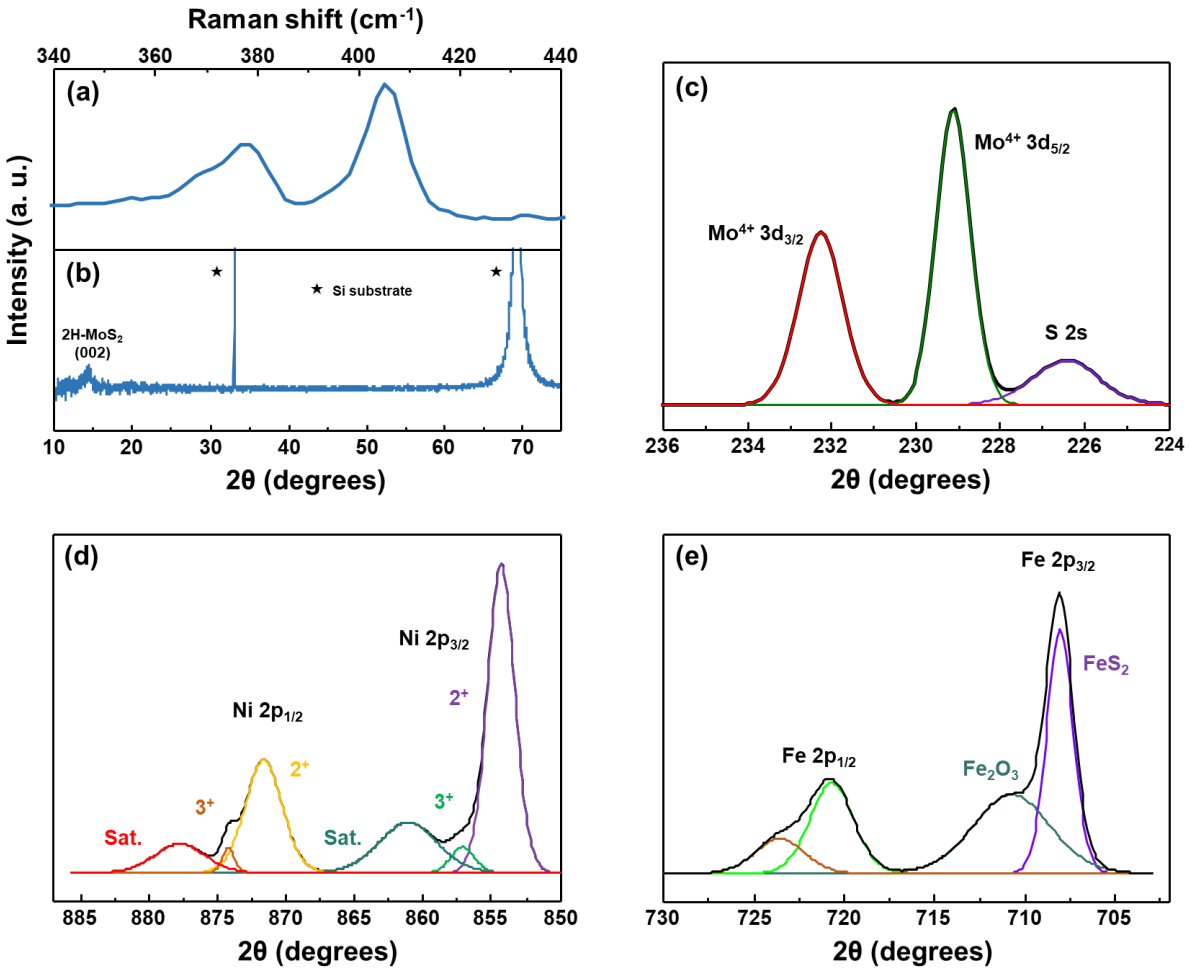

Fig. S12. (**a**) Raman spectra and (**b**) XRD patterns of the F1N9S/VMS/*p*-Si photocathode after the stability test. XPS analysis of the F1N9S/VMS/*p*-Si photocathode after the stability test for (c) Mo 3*d*, (d) Ni 2*p*, and (e) Fe 2*p*.

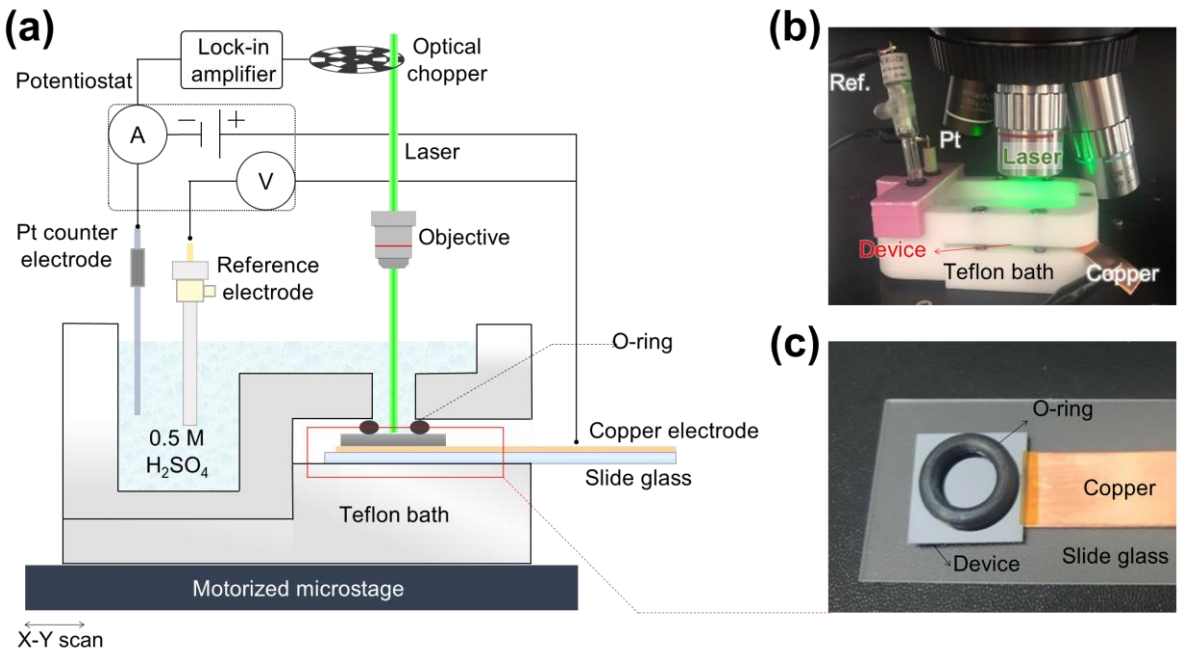

Fig. S13. (**a**) Schematic of the SPECM measurement setup, combining scanning photocurrent microscopy with a standard three-electrode electrochemical measurement. A copper electrode contacting the device, Pt, and the saturated calomel electrode are used as the working, counter and reference electrodes, respectively. The home-designed reaction bath is illuminated by a 532-nm laser from above. (**b**) Photograph of the measurement with a 532-nm laser and mapping stage. (**c**) Photograph of the fabricated device on slide glass with O-ring. The device is electrically connected to a copper electrode through an InGa eutectic alloy and silver paste.

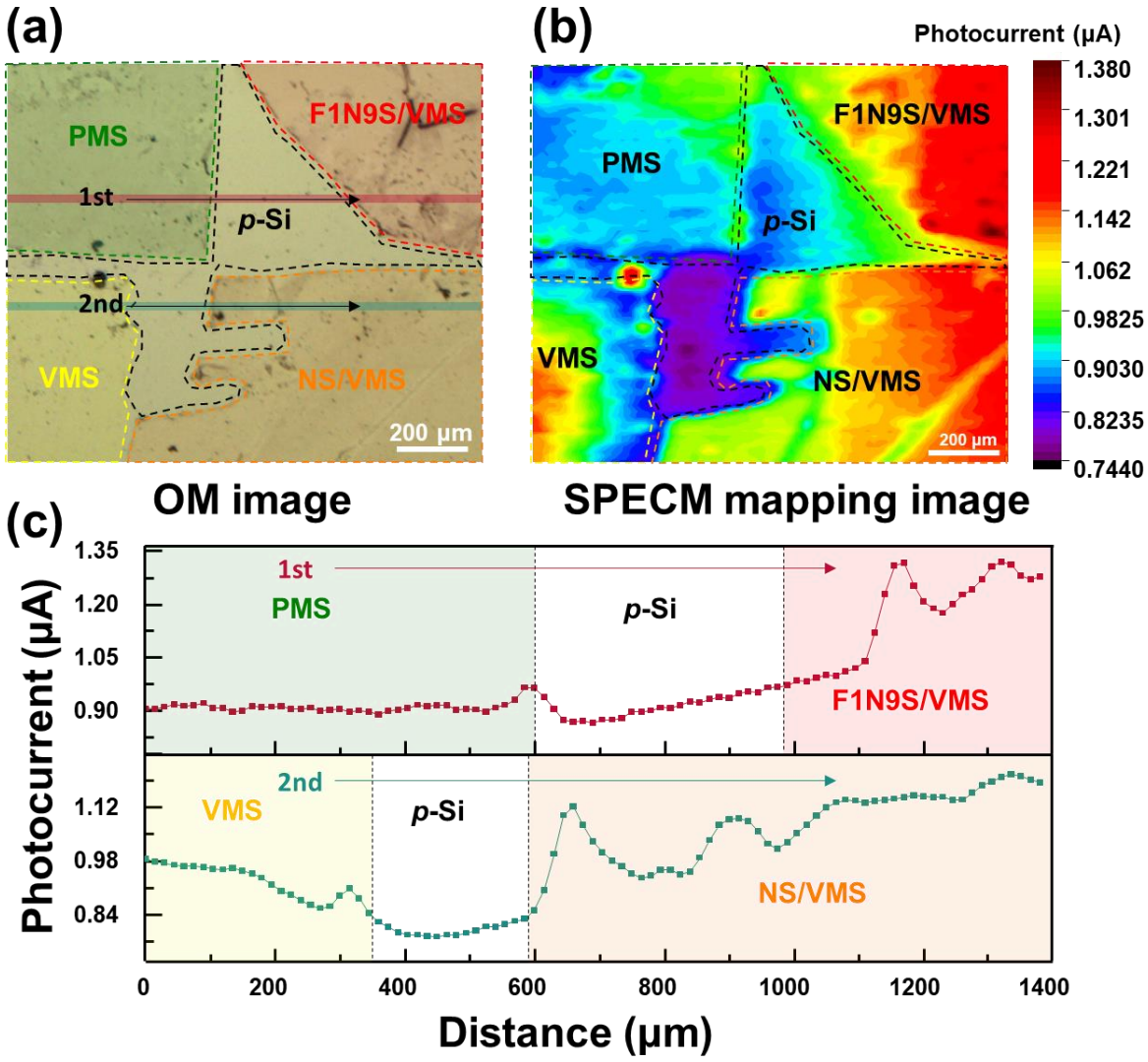

Fig. S14. (**a**) Optical image of the fabricated device. (**b**) Photocurrent mapping image of the device at -0.1 V vs. RHE. Scale bars in (a) and (b) are 200 μm. (**c**) Corresponding line profiles of photocurrent along the solid lines in (a). Red (1st) and green (2nd) line profiles are obtained along the red (1st) and green (2nd) solid lines in (a), respectively. Red, green, orange and yellow shaded regions indicate F1N9S/VMS, PMS, NS/VMS and VMS, respectively.

Table S1. Calculated work function and $E_V - E_F$ values of PMS/*p*-Si, VMS/*p*-Si, and FNS NPs/*p*-Si photocathodes.

Photocathode	Work function (eV)	E_F – VBM (eV)
Au	5.10	0
***p*-Si**	4.70	0.40
PMS	4.34	1.36
VMS	4.36	1.12
NS (Ni_3S_2)	4.31	0.033
F1N9S	4.32	0.030
F5N5S	4.29	0.17
FS (FeS_2)	4.32	0.38

Table S2. Comparison of experimental results with previously reported transition metal sulfide catalysts.

Electrocatalyst	Type	Overpotential (mV) @ 10 mA cm^{-2}	Tafel slope (mV dec^{-1})	Ref	Electrolyte
F1N9S/VMS	Thin film	**106**	**68.5**	**This study**	**0.5 M H_2SO_4**
Defective-rich MoS_2		208	160	[1]	0.5 M H_2SO_4
Au nanorods on MoS_2 nanosheet		220	71	[2]	0.5 M H_2SO_4
Vertically aligned MoS_2 nanosheets with graphene		421	84	[3]	0.5 M H_2SO_4
Core-shell MoO_3-MoS_2 nanowires	Nanostructure	~175	~55	[4]	0.5 M H_2SO_4
Ni-Co-MoS_2 nanoboxes		155	51	[5]	0.5 M H_2SO_4
P, Se-co-doped MoS_2 nanosheets on CNTs		110	49	[6]	0.5 M H_2SO_4
MoS_2 nanosheets on TiN nanorods		146-195	44.8-65.6	[7]	0.5 M H_2SO_4
CoS_2-MoS_2/CNTs		70	67	[8]	0.5 M H_2SO_4
Co-doped MoS_2 nanosheets on Carbon		90	50	[9]	0.5 M H_2SO_4
Cu nanoparticle deposited MoS_2 nanoflowers on GO sheet		126	90	[10]	0.5 M H_2SO_4
N-doped Cu_2S/MoS_2 nanorod arrays		91	41	[11]	1 M KOH
Ni_xS_y-MoS_2 hybrid microspheres	Microstructure	~290	55.6	[12]	0.5 M H_2SO_4

Supporting Information References

[1] Y. Li, K. Yin, L. Wang, X. Lu, Y. Zhang, Y. Liu, D. Yan, Y. Song, S. Luo, Engineering MoS2 nanomesh with holes and lattice defects for highly active hydrogen evolution reaction, Applied Catalysis B: Environmental, 239 (2018) 537-544.

[2] Y. Shi, J. Wang, C. Wang, T.-T. Zhai, W.-J. Bao, J.-J. Xu, X.-H. Xia, H.-Y. Chen, Hot electron of Au nanorods activates the electrocatalysis of hydrogen evolution on MoS2 nanosheets, J. Am. Chem. Soc., 137 (2015) 7365-7370.

[3] P. Gnanasekar, D. Periyanagounder, J. Kulandaivel, Vertically aligned MoS 2 nanosheets on graphene for highly stable electrocatalytic hydrogen evolution reactions, Nanoscale, 11 (2019) 2439-2446.

[4] Z. Chen, D. Cummins, B.N. Reinecke, E. Clark, M.K. Sunkara, T.F. Jaramillo, Core–shell MoO3–MoS2 nanowires for hydrogen evolution: a functional design for electrocatalytic materials, Nano Lett., 11 (2011) 4168-4175.

[5] X.Y. Yu, Y. Feng, Y. Jeon, B. Guan, X.W. Lou, U. Paik, Formation of Ni–Co–MoS_2 nanoboxes with enhanced electrocatalytic activity for hydrogen evolution, Adv. Mater., 28 (2016) 9006-9011.

[6] T. Zhu, J. Ding, Q. Shao, Y. Qian, X. Huang, P, Se-Codoped MoS2 Nanosheets as Accelerated Electrocatalysts for Hydrogen Evolution, ChemCatChem, 11 (2019) 689-692.

[7] M. Yu, S. Zhao, H. Feng, L. Hu, X. Zhang, Y. Zeng, Y. Tong, X. Lu, Engineering thin MoS_2 nanosheets on TiN nanorods: advanced electrochemical capacitor electrode and hydrogen evolution electrocatalyst, ACS Energy Lett., 2 (2017) 1862-1868.

[8] Y.-R. Liu, W.-H. Hu, X. Li, B. Dong, X. Shang, G.-Q. Han, Y.-M. Chai, Y.-Q. Liu, C.-G. Liu, Facile one-pot synthesis of CoS2-MoS2/CNTs as efficient electrocatalyst for hydrogen evolution reaction, Appl. Surf. Sci., 384 (2016) 51-57.

[9] X. Dai, K. Du, Z. Li, M. Liu, Y. Ma, H. Sun, X. Zhang, Y. Yang, Co-doped MoS2 nanosheets with the dominant CoMoS phase coated on carbon as an excellent electrocatalyst for hydrogen evolution, ACS Appl. Mater. Interfaces, 7 (2015) 27242-27253.

[10] F. Li, L. Zhang, J. Li, X. Lin, X. Li, Y. Fang, J. Huang, W. Li, M. Tian, J. Jin, R. Li, Synthesis of Cu–MoS2/rGO hybrid as non-noble metal electrocatalysts for the hydrogen evolution reaction, J. Power Sources, 292 (2015) 15-22.

[11] X. Wang, J. Wang, X. Zhang, Q. Tian, M. Liu, N. Cai, Y. Xue, W. Chen, W. Li, F. Yu, Nitrogen-Doped Cu2S/MoS2 Heterojunction Nanorod Arrays on Copper Foam for Efficient Hydrogen Evolution Reaction, ChemCatChem, 11 (2019) 1354-1361.

[12] W. Cui, C. Ge, Z. Xing, A.M. Asiri, X. Sun, NixSy-MoS2 hybrid microspheres: One-pot hydrothermal synthesis and their application as a novel hydrogen evolution reaction electrocatalyst with enhanced activity, Electrochim. Acta, 137 (2014) 504-510.